

The future of quantum computing in High Energy Physics

Author 1^{a,c,*}, Author 2^a, Author 3^b, Author 4^b, Author 5^c, Author 6^a and Author 7^{b,*}

^aInstitute of High Energy Physics, University of Chinese Academy of Sciences, 19B Yuquan Road, Shijingshan District, Beijing 100049, China

^bSchool of Physics, Peking University, Chengfu Road, Haidian District, Beijing 100871, China

^cSchool of Physics and Institute for Collider Particle Physics, University of the Witwatersrand, Johannesburg, Wits 2050, South Africa

ARTICLE INFO

Keywords:

Quantum computing
High Energy Physics
Machine Learning

ABSTRACT

This is a abstract. Nulla malesuada porttitor diam. Donec felis erat, congue non, volutpat at, tincidunt tristique, libero. Vivamus viverra fermentum felis. Donec nonummy pellentesque ante. Phasellus adipiscing semper elit. Proin fermentum massa ac quam. Sed diam turpis, molestie vitae, placerat a, molestie nec, leo. Maecenas lacinia. Nam ipsum ligula, eleifend at, accumsan nec, suscipit a, ipsum. Morbi blandit ligula feugiat magna. Nunc eleifend consequat lorem. Sed lacinia nulla vitae enim. Pellentesque tincidunt purus vel magna. Integer non enim. Praesent euismod nunc eu purus. Donec bibendum quam in tellus. Nullam cursus pulvinar lectus. Donec et mi. Nam vulputate metus eu enim. Vestibulum pellentesque felis eu massa.

1. Introduction

The discovery of the Higgs boson [2, 5] by the ATLAS and CMS experiments at the Large Hadron Collider (LHC) in 2012 was a major milestone in particle physics. It confirmed the fundamental particle spectrum of the Standard Model and opened a new way to refine our understanding of particle physics. Since then, the LHC experiments have performed extensive studies on the Higgs boson properties: clues for new physics would emerge if any measurement disagrees with the Standard Model prediction. Furthermore, Higgs factories based on lepton colliders have been proposed to perform more precision measurements of the Higgs boson properties and study deeper structure of particle physics. The Circular Electron-Positron Collider (CEPC), proposed by China, is one of the proposed Higgs factories. It will be located in a tunnel with a circumference of approximately 100 km and collide electron-positron pairs at a center-of-mass energy of up to 250 GeV.

Machine learning has enjoyed widespread success in detector simulation, particle reconstruction and data analyses of experimental particle physics and greatly enhances the ability to achieve physics discovery. For instance, the ATLAS and CMS experiments use machine learning algorithms such as boosted decision trees and deep neural networks to help separate signal from background in the observation for the Higgs boson production in association with a top quark pair ($t\bar{t}H$), which directly establishes the Higgs boson couplings to the top quarks [3, 4].

Another important tool for experimental particle physics could be quantum machine learning. It uses quantum computing to perform machine learning tasks, which typically tackle large data dimensions. Using qubits instead of classical bits, quantum machine learning enables effective operations in high-dimensional quantum state spaces. Therefore, it could possibly provide fast computing speed and better learning ability compared to classical machine learning.

As an example of quantum machine learning, a support vector machine algorithm with a quantum kernel estimator (QSVM-Kernel) [7, 10] encodes classical data into quantum state space and makes accurate classifications for certain artificial data sets.

In recent years, the field of quantum computing has developed rapidly. Superconducting quantum computers and optical quantum computers have been successfully fabricated and they have demonstrated capabilities far beyond today's supercomputers in certain computing tasks [? ?]. In the next decades, this field is likely to further increase the number of qubits, improve execution time, and reduce device noise for the quantum computers. These developments will lay a foundation for the practical application of quantum computing.

To utilize potential quantum advantage for future particle physics research, there have already been proof-of-principle studies that apply quantum machine learning algorithms to detector simulation, particle reconstruction and data analyses. For example, the QSVM-Kernel algorithm has been employed in a $t\bar{t}H$ physics analysis at the LHC using both quantum computer simulators and superconducting quantum computer hardware [1]. This study confirms that the quantum machine learning algorithm has the ability to separate signal from background for certain realistic physics data sets. However, further improvements on both quantum algorithms and quantum devices are still required before the actual use of quantum machine learning in particle physics experiments.

In this study, we focus on applying the QSVM-Kernel algorithm to a physics analysis that measures ZH (Higgs boson production in association with a Z boson) at the CEPC. Using quantum computer simulators, we pursue quantum algorithm designs that are more suitable for particle physics data analyses. On the other hand, we validate the performance of the QSVM-Kernel algorithm using superconducting quantum computer hardware provided by Origin Quantum, a quantum technology company in China. We expect improved quantum machine learning algorithms and quantum computer hardware could facilitate physics discovery in

*Corresponding author

✉ Author 1@mail (A. 1); Author 7@mail (A. 7)
ORCID(s): ORCID (A. 1)

the interesting data produced by the CEPC.

2. Physics Analysis

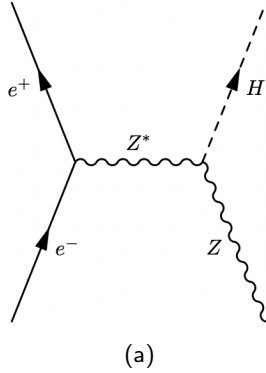


Figure 1: Representative Feynman diagrams for (a) $e^+e^- \rightarrow ZH$ production.

The CEPC will produce over one million Higgs boson events. The large statistics, together with the clean final states of electron-positron collisions, will allow the CEPC experiments to measure the Higgs boson properties with precision far beyond that at the LHC. The main Higgs production mode at the CEPC is $e^+e^- \rightarrow ZH$ (ZH associate production). See Figure 1 for a representative Feynman diagram for ZH production.

$e^+e^- \rightarrow ZH$ events can be tagged using the mass of the system recoiling against the Z boson (“recoil mass”), calculated using the four momenta of the electron-positron pair and the Z boson. Combining this method with measurements in individual Higgs decay channels will allow for model-independent measurements of both $e^+e^- \rightarrow ZH$ production cross section and Higgs decay branching ratios, which is not feasible at the LHC. These measurements will extract information on Higgs boson couplings to other fundamental particles and provide sensitive probes to physics beyond the Standard Model.

In our study, we focus on the $H \rightarrow \gamma\gamma, Z \rightarrow q\bar{q}$ decay mode of the $e^+e^- \rightarrow ZH$ process. Events are required to have two photon candidates retained as the $H \rightarrow \gamma\gamma$ candidate, as well as two jets retained as the $Z \rightarrow q\bar{q}$ candidate. (mention other selection cuts?) Although the diphoton decay of the Higgs boson has a small branching ratio in the SM, the two photons can be well identified and measured, which boosts the precision in this channel. The main SM background process in this analysis is the $e^+e^- \rightarrow (Z/\gamma^*)\gamma\gamma$ process where the γ 's originate from initial or final state radiation.

The Higgs signal and the SM background events are generated with WHIZARD. The generated events are passed to MokkaC for detector simulation and event reconstruction: the Higgs signal samples are processed with the Geant4 full simulation, while the SM background samples are processed with a dedicated fast simulation tool. (add references.)

To separate signal from background, we construct classifiers based on (either classical or quantum) machine learning algorithms. The kinematic features utilized by these classifiers include: the azimuthal separation between the two photons $\Delta\phi(\gamma\gamma)$, the minimum angular distance between a photon and a jet $\min(\Delta R(\gamma, j))$, energy of the diphoton system $e_{\gamma\gamma}$, momentum of the diphoton system $p_{\gamma\gamma}$, difference in momentum between the diphoton system and dijet system $\Delta P_{\gamma\gamma, jj}$, and recoil mass of the dijet system M_{recoil}^{jj} . The outputs of these classifiers can be used to create event categories and therefore improve the analysis sensitivity.

3. Quantum algorithm

The support vector machine (SVM) algorithm with various kernel estimators has been one of the best known machine learning algorithms for classification problems such as identifying small signal from large background. A quantum version of the SVM algorithm with a quantum kernel estimator (QSVM-Kernel) was proposed to leverage high-dimensional quantum state space for identification accuracy and computational speed. This QSVM-Kernel algorithm is employed and investigated in our study. Conceptually, the training phase of this algorithm can be divided into three following steps.

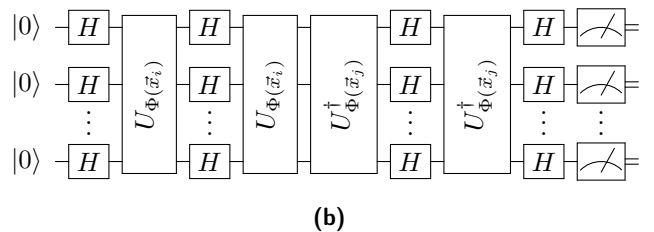
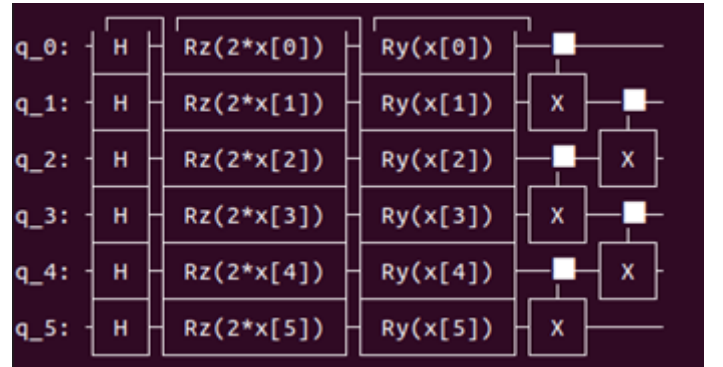


Figure 2: (a) Quantum circuit of the quantum feature map $U_{\Phi(\vec{x})}$ in our study. It is constituted by single-qubit rotation gates (H , R_z and R_y) and two-qubit CNOT entangling gates. (b) Quantum circuit for evaluating the kernel entry for data events \vec{x}_i and \vec{x}_j in our study.

A. Map classical data

For each classical data point in the training sample, we use \vec{x} to denote the vector of its kinematic features and use $y \in \{0, 1\}$ to denote its event class (0 for background and 1 for

signal). The QSVM-Kernel algorithm maps \vec{x} to a quantum state of N qubits, which is a superposition of 2^N eigenstates. Initially, all the N qubits are in the $|0\rangle$ state. A quantum feature map circuit $\mathcal{U}_{\Phi(\vec{x})}$, which represents a unitary transformation, is applied to the N qubits and results in a new quantum state:

$$|\Phi(\vec{x})\rangle = \mathcal{U}_{\Phi(\vec{x})}|0^{\otimes N}\rangle \quad (1)$$

The quantum feature map circuit decides how the 2^N dimensional quantum state space will be utilized and the choice of the circuit is essential for the performance of the QSVM-kernel algorithm. The quantum feature map $\mathcal{U}_{\Phi(\vec{x})}$ in our study, shown in Figure 2 (a), is constituted by single-qubit rotation gates (H , Rz and Ry) and two-qubit CNOT entangling gates. Given an input feature vector \vec{x} (where x_k denotes the k^{th} element of \vec{x}), the k^{th} qubit will be sequentially rotated by an Hadamard (H) gate to the $(\frac{0+1}{\sqrt{2}})$ state, rotated by a Rz gate for $2 * x_k$ around the z axis of the Bloch sphere, and rotated by a Ry gate for x_k around the y axis by x_k . To avoid long-depth circuits on noisy intermediate scale quantum computers, CNOT entangling gates (which operate the target qubits according to the state of the control qubits) are arranged in an alternating manner: in the first layer, the k^{th} CNOT gate takes the $2 * k - 1$ qubit as the control qubit and takes the $2 * k$ qubit as the target qubit; and in the second layer, the k^{th} CNOT gate takes the $2 * k$ qubit as the control qubit and takes the $2 * k + 1$ qubit as the target qubit.

B. Quantum Kernel estimation

The QSVM-Kernel algorithm defines the “kernel entry” between any two data points \vec{x}_i and \vec{x}_j as the square of the inner product of their quantum states.

$$k(\vec{x}_i, \vec{x}_j) = |\langle \Phi(\vec{x}_i) | \Phi(\vec{x}_j) \rangle|^2 \quad (2)$$

The mathematical implication of the kernel entry is the distance between the two data points in the high-dimensional quantum state space.

It can be shown that

$$k(\vec{x}_i, \vec{x}_j) = |\langle 0^{\otimes N} | \mathcal{U}_{\Phi(\vec{x}_i)}^\dagger \mathcal{U}_{\Phi(\vec{x}_j)} | 0^{\otimes N} \rangle|^2 \quad (3)$$

Therefore the kernel entry can be calculated using just N qubits on a quantum computer, by preparing the $\mathcal{U}_{\Phi(\vec{x}_i)}^\dagger \mathcal{U}_{\Phi(\vec{x}_j)} | 0^{\otimes N} \rangle$ state and measuring it in the standard basis with a sufficient number of measurement shots. The frequency of obtaining the $|0^{\otimes N}\rangle$ state in the measurement outputs is taken as the value of the kernel entry. Except the $\mathcal{U}_{\Phi(\vec{x})}$ design, the quantum circuit for calculating the kernel entries is the same as Ref [7] and given in Figure 2 (b).

C. Finding separating hyperplane

Using the kernel entries, the QSVM-Kernel algorithm looks for a hyperplane that separate signal from background in the quantum state space:

$$\left(\sum_{i=1}^t \alpha_i y_i k(\vec{x}_i, \vec{x}) + b \right) = 0 \quad (4)$$

where t is the size of the training dataset, i is the index of the training data points, and (α_i, b) are parameters to be optimized. The optimization of the separating hyperplane takes the same procedure as for the classical SVM, and is done in a classical computer.

In the testing phase of the QSVM-Kernel algorithm, given any new data point \vec{x}' , the kernel entry between \vec{x}' and each training data point is calculated on a quantum computer. Then, on a classical computer and as for the classical SVM, the data point \vec{x}' is classified as “signal” or “background” based on the separating hyperplane, i.e. the sign of $(\sum_{i=1}^t \alpha_i y_i k(\vec{x}_i, \vec{x}') + b)$. In addition, the probability for the data point \vec{x}' to be in the signal class can be evaluated and used as a continuous discriminant.

4. Results from Quantum Computer Simulators

We employ the QSVM-Kernel algorithm using 6 qubits on the *Statevector Simulator* from the IBM Quantum framework [8] and the *Full-Amplitude Simulator* from the Origin QPanda framework [?]. Running on classical computers, these tools simulate quantum computers by computing the wavefunction of the qubits as the quantum gates are executed, and outputs the “true” probabilities for each eigenstate when measurements are performed. In our usage of the quantum computer simulators, hardware noises are not considered. These choices lead to reasonable computational speed that allows us to explore large datasets. For a $e^+e^- \rightarrow ZH$ analysis dataset of size M , we prepare $\frac{1}{2}M$ simulated signal events and $\frac{1}{2}M$ simulated background events. We split the analysis dataset to a training sample and a test sample: the training sample consists of $\frac{1}{3}M$ simulated signal events and $\frac{1}{3}M$ simulated background events, and the test sample consists of $\frac{1}{6}M$ simulated signal events and $\frac{1}{6}M$ simulated background events. To evaluate the statistical fluctuation level, we perform this splitting several times, train and test a QSVM-Kernel classifier for each shuffle, and report the average and variation of the results. The SVM regularization hyperparameter for QSVM-Kernel is optimized using a cross-validation procedure. With the same datasets, a classical SVM [6?] classifier with the RBF kernel is trained using the scikit-learn package [9], which serves as the classical counterpart for the QSVM-Kernel classifier. Using the same cross-validation procedure as for QSVM-Kernel, we extensively optimize the SVM regularization hyperparameter and the RBF kernel’s γ parameter.

We first build QSVM-Kernel and classical SVM classifiers for a $e^+e^- \rightarrow ZH$ analysis dataset of 12500 events. To study the performance for the machine learning-based models, we plot Receiver Operating Characteristic (ROC) curves, which show background rejection (in y-axis) as a function of signal efficiency (in x-axis) using the continu-

ous discriminants of the classifiers. The ROC curves for the QSVM-Kernel algorithm (blue) and the classical SVM algorithm (black) are overlaid in Figure 3 (a). The IBM *Statevector Simulator* and the Origin *Full-amplitude Simulator* produce identical ROC curves and are therefore shown together. Additionally, we calculate the areas under the ROC curves (AUCs) for the classifiers, which is a quantitative metric for evaluating performances of machine learning applications. The AUC of the QSVM-Kernel classifier is found to be $0.940 \pm$, compared to $0.946 \pm$ for the classical SVM classifier. The comparison with the ROC curves and AUCs indicates that the quantum SVM algorithm provides similar separation power with its classical counterpart in the $e^+e^- \rightarrow ZH$ analysis dataset.

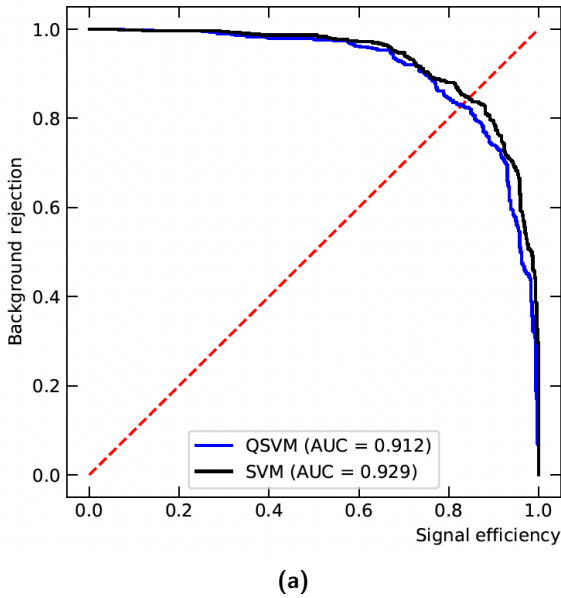


Figure 3: ROC curves of machine learning classifiers using the $e^+e^- \rightarrow ZH$ analysis dataset of 12500 events. (a) overlays the results of the QSVM-Kernel algorithm (blue) and the classical SVM algorithm (black).

Furthermore, we construct QSVM-Kernel and classical SVM classifiers for the $e^+e^- \rightarrow ZH$ analysis with different dataset sizes from 50 to 12500 events. Figure 4 (a) overlays the AUC results of the QSVM-Kernel and the classical SVM as a function of the dataset size. Figure 4 (b) further shows the difference in AUC between the QSVM-Kernel algorithm and the classical SVM algorithm, again as a function of the dataset size. The quoted AUCs are the mean of the AUCs of several shuffles of a dataset and the quoted errors are the standard deviation for the AUCs of the shuffles. As shown in the figure, in terms of separating signal from background for the $e^+e^- \rightarrow ZH$ analysis, both algorithms improves the performances with larger dataset size, and for up to 12500 events, the QSVM-Kernel algorithm performs similarly with the classical SVM algorithm.

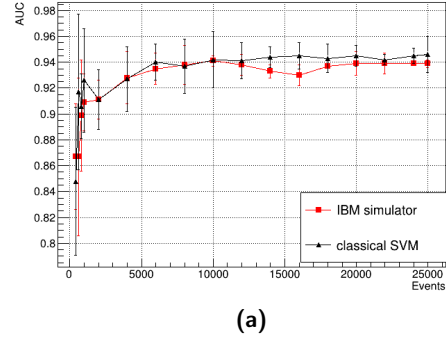


Figure 4: The AUCs of the QSVM-Kernel and classical SVM classifiers for the $e^+e^- \rightarrow ZH$ analysis with different dataset sizes from 50 to 12500 events. (a) overlays the AUC results of the QSVM-Kernel and the classical SVM as a function of the dataset size. (b) shows the difference in AUC between the QSVM-Kernel algorithm and the classical SVM algorithm, again as a function of the dataset size. The quoted AUCs are the mean of the AUCs of several shuffles of the dataset and the quoted errors are the standard deviations for the AUCs of the shuffles.

5. Results from Quantum Computer Hardware

In addition to the studies with noiseless quantum computer simulators, we further investigate the QSVM-Kernel algorithm with noisy quantum computer hardware, the 7-qubit Nairobi quantum computer from the IBM company and the 6-qubit Wuyuan quantum computer from the Origin Quantum company. The core of both quantum computers is a superconducting quantum chip system. We employed 6 qubits on both the IBM Nairobi and Origin Wuyuan quantum computers. The topology structures of the 6 qubits in the quantum chip systems are shown in Figure 5. The quantum circuits on the quantum computer hardware are identical to those on the quantum computer simulators. Each quantum circuit was executed and measured for 10000 times to allow sufficient statistical precision in evaluating kernel entries. Due to the currently long execution time of the quantum computer hardware, here we analyze a smaller $e^+e^- \rightarrow ZH$ analysis dataset consisting of 100 training events and 100 test events. The needed time to complete the training and test for this dataset is xxx minutes for IBM Nairobi quantum computer and yyy minutes for Origin Wuyuan quantum computer.

We plot the ROC curve of the QSVM-Kernel classifiers from the IBM Nairobi and Origin Wuyuan quantum computer hardware, as shown in Figure 6. The ROC curve from the *Statevector Simulator* with the same $e^+e^- \rightarrow ZH$ analysis dataset is overlaid for comparison. The AUC reaches 0.894 from the Origin Wuyuan quantum computer hardware and 0.838 from the IBM Nairobi quantum computer hard-

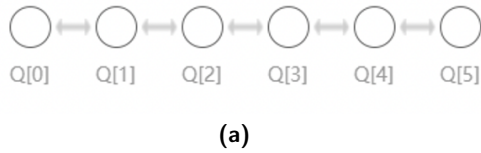


Figure 5: The topology structure of the 6 qubits in IBM Nairobi (a) and Origin Wuyuan (b) quantum chip system.

ware, compared to 0.925 from the *StatevectorSimulator*. We find that the separation power provided by the current quantum computer hardware is approaching that by the noiseless quantum computer simulator. The remaining difference and the difference between IBM Nairobi and Origin Wuyuan results are related to the quantum hardware noises and statistical fluctuations at the time of executing the hardware tasks.

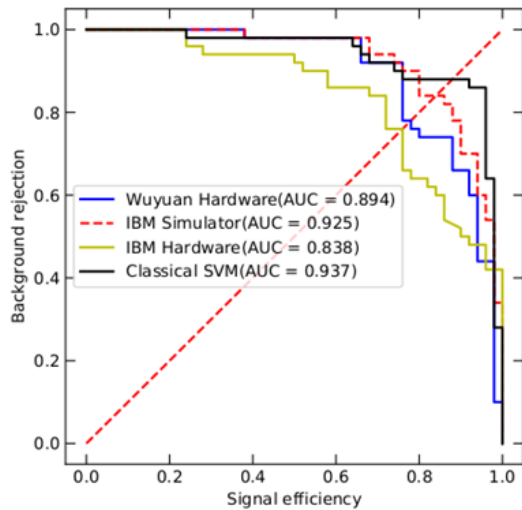


Figure 6: The ROC curve of the QSVM-Kernel classifiers from the IBM Nairobi quantum computer hardware, the Origin Wuyuan quantum computer hardware and the *StatevectorSimulator* with the same $e^+e^- \rightarrow ZH$ analysis dataset.

6. Conclusion

In this study, we have employed the QSVM-Kernel algorithm to study Higgs boson production in association with a Z boson at the CEPC, a Higgs factory proposed by China to study deeper structure of particle physics. QSVM-Kernel is a quantum machine learning algorithm that leverages high-dimensional quantum state space for identifying signal from background. Using quantum computer simulators, we have optimized the quantum circuits of the QSVM-Kernel algorithm for use in our physics data analysis and obtained similar classification accuracy to the classical SVM algorithm for different dataset sizes from 50 events to 12500 events.

On the other hand, we have validated the QSVM-Kernel algorithm using superconducting quantum computer hardware from both IBM and Origin (a quantum technology company in China), where the classification accuracy is approaching noiseless quantum computer simulators.

Looking into the future, given the momentum in the field of quantum technology, we expect to see further improved quantum machine learning algorithms and quantum computer hardware. With these improvements, particle physicists could better handle high dimensions and large size of physics datasets from future particle colliders, which will increase the chances to achieve discovery of new physics phenomena.

Conflict of interest

Acknowledgements

Author contributions

A. Appendix

References

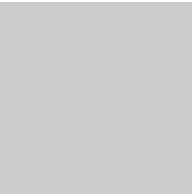
- [1] et al., S.L.W., 2021. Application of quantum machine learning using the quantum kernel algorithm on high energy physics analysis at the LHC. *Physical Review Research* 3, 033221.
- [2] ATLAS Collaboration G. Aad et al., 2012. Observation of a new particle in the search for the standard model Higgs boson with the ATLAS detector at the LHC. *Physics Letters B* 716, 1–29.
- [3] ATLAS Collaboration, M. Aaboud et al., 2018. Observation of Higgs boson production in association with a top quark pair at the LHC with the ATLAS detector. *Physics Letters B* 784, 173–191.
- [4] CMS Collaboration, A. M. Sirunyan et al., 2018. Observation of $t\bar{t}H$ production. *Physical Review Letters* 120, 231801.
- [5] CMS Collaboration, S. Chatrchyan et al., 2012. Observation of a new boson at a mass of 125 GeV with the CMS experiment at the LHC. *Physics Letters B* 716, 30–61.
- [6] Cortes, C., Vapnik, V., 1995. Support-vector networks. *Machine learning* 20, 273–297.
- [7] Havlíček, V., Córcoles, A.D., Temme, K., Harrow, A.W., Kandala, A., Chow, J.M., Gambetta, J.M., 2019. Supervised learning with quantum-enhanced feature spaces. *Nature* 567, 209–212.
- [8] MD SAJID ANIS et al., 2021. Qiskit: An open-source framework for quantum computing. doi:10.5281/zenodo.2573505.
- [9] Pedregosa, F., Varoquaux, G., Gramfort, A., Michel, V., Thirion, B., Grisel, O., Blondel, M., Prettenhofer, P., Weiss, R., Dubourg, V., et al., 2011. Scikit-learn: Machine learning in python. *Journal of machine learning research* 12, 2825–2830.
- [10] Schuld, M., Killoran, N., 2019. Quantum machine learning in feature Hilbert spaces. *Physical Review Letters* 122, 040504.

Lorem ipsum dolor sit amet, consectetur adipiscing elit. Ut purus elit, vestibulum ut, placerat ac, adipiscing vitae, felis. Curabitur dictum gravida mauris. Nam arcu libero, nonummy eget, consectetur id, vulputate a, magna. Donec vehicula augue eu neque. Pellentesque habitant morbi tristique senectus et netus et malesuada fames ac turpis egestas. Mauris ut leo. Cras viverra metus rhoncus sem. Nulla et lectus vestibulum urna fringilla ultrices. Phasellus eu tellus sit amet tortor gravida placerat. Integer sapien est, iaculis in, pretium quis, viverra ac, nunc. Praesent eget sem vel leo ultrices bibendum. Aenean faucibus. Morbi dolor nulla,

malesuada eu, pulvinar at, mollis ac, nulla. Curabitur auctor semper nulla. Donec varius orci eget risus. Duis nibh mi, congue eu, accumsan eleifend, sagittis quis, diam. Duis eget orci sit amet orci dignissim rutrum.



Lorem ipsum dolor sit amet, consectetur adipiscing elit. Ut purus elit, vestibulum ut, placerat ac, adipiscing vitae, felis. Curabitur dictum gravida mauris. Nam arcu libero, nonummy eget, consectetur id, vulputate a, magna. Donec vehicula augue eu neque. Pellentesque habitant morbi tristique senectus et netus et malesuada fames ac turpis egestas. Mauris ut leo. Cras viverra metus rhoncus sem. Nulla et lectus vestibulum urna fringilla ultrices. Phasellus eu tellus sit amet tortor gravida placerat. Integer sapien est, iaculis in, pretium quis, viverra ac, nunc. Praesent eget sem vel leo ultrices bibendum. Aenean faucibus. Morbi dolor nulla, malesuada eu, pulvinar at, mollis ac, nulla. Curabitur auctor semper nulla. Donec varius orci eget risus. Duis nibh mi, congue eu, accumsan eleifend, sagittis quis, diam. Duis eget orci sit amet orci dignissim rutrum.



Lorem ipsum dolor sit amet, consectetur adipiscing elit. Ut purus elit, vestibulum ut, placerat ac, adipiscing vitae, felis. Curabitur dictum gravida mauris. Nam arcu libero, nonummy eget, consectetur id, vulputate a, magna. Donec vehicula augue eu neque. Pellentesque habitant morbi tristique senectus et netus et malesuada fames ac turpis egestas. Mauris ut leo. Cras viverra metus rhoncus sem. Nulla et lectus vestibulum urna fringilla ultrices. Phasellus eu tellus sit amet tortor gravida placerat. Integer sapien est, iaculis in, pretium quis, viverra ac, nunc. Praesent eget sem vel leo ultrices bibendum. Aenean faucibus. Morbi dolor nulla, malesuada eu, pulvinar at, mollis ac, nulla. Curabitur auctor semper nulla. Donec varius orci eget risus. Duis nibh mi, congue eu, accumsan eleifend, sagittis quis, diam. Duis eget orci sit amet orci dignissim rutrum.